

Phase retrieval and saddle-point optimization

Stefano Marchesini*

*Lawrence Livermore National Laboratory, 7000 East Ave., Livermore, CA 94550-9234, USA and
Center for Biophotonics Science and Technology, University of California,
Davis, 2700 Stockton Blvd., Ste 1400, Sacramento, CA 95817, USA*

Iterative algorithms with feedback are amongst the most powerful and versatile optimization methods for phase retrieval. Among these, the hybrid input-output algorithm has demonstrated practical solutions to giga-element nonlinear phase retrieval problems, escaping local minima and producing images at resolutions beyond the capabilities of lens-based optical methods. Here the input-output iteration is improved by a lower dimensional subspace saddle-point optimization.

© 2018 Optical Society of America

OCIS codes: 100.5070 100.3190

1. Introduction

Phase retrieval is one of the toughest challenges in optimization, requiring the solution of large-scale, nonlinear, non-convex and non-smooth constrained problems. Despite such challenge, efficient algorithms are being used in astronomical imaging, electron microscopy, lensless x-ray imaging (diffraction microscopy) and x-ray crystallography, substituting lenses and other optical elements in the image-forming process.

In diffraction microscopy, photons scattered from an object (diffraction pattern) are recombined solving the giant puzzle of placing millions of waves into a limited area. X-ray diffraction microscopy [1] has successfully been applied to image objects as complex as biological cells [2], quantum dots [3], nanocrystals [4] and nanoscale aerogel structures [5]. Nanofabricated test objects were reconstructed computationally in 3D with several millions 10 nm resolution elements [6], other test patterns were captured in the fastest flash image ever recorded at suboptical resolution [7].

These experimental methods (see e.g. [8] for a review) are being developed thanks to advances in optimization techniques, primarily the introduction of a control-feedback method proposed by Fienup (Hybrid Input Output-HIO [9, 10]). The important theoretical insight that these iterations may be viewed as projections in Hilbert space [11, 12] has allowed theoreticians to analyze and improve on the basic HIO algorithm [13, 14, 15, 16]. More recently Elser et al. [17, 18] connected the phase retrieval problem to other forms of “puzzles”, demonstrating performances of their Difference Map algorithm [13] (a generalization of HIO) often superior to dedicated optimization packages in problems as various as graph coloring, protein folding, sudoku and

spin glass states. Rather than performing a local optimization of a constrained problem, the common theme of these algorithms is that they seek a solution to a different type of fixed point, the saddle-point of the difference between antagonistic error metrics [19] with respect to the feasible and unfeasible spaces defined by the constraints.

Here each input-output iteration is improved by a lower dimensional subspace optimization of this saddle-point problem along the steepest descent-ascent directions defined by the constraints. This lower dimensional optimization (performed here by Newton methods) is analogous to one dimensional line searches of gradient based methods, used to avoid overshooting and undershooting in new search directions and providing faster and more reliable algorithms.

The first sections introduce the phase retrieval problem and the saddle point optimization method, reformulating the HIO algorithm in terms of gradients and constraints (see [19] for further details). Sections 5 describe this lower dimensional optimization. Benchmarks performed on a simple simulated test pattern are described in the Sec. 6.

2. Phase retrieval problem

When we record the diffraction pattern intensity of light scattered by an object, the phase information is lost. Apart from normalization factors, an object with density $\rho(\mathbf{r})$, \mathbf{r} being the coordinates in the *object* (or *real*) space, generates a diffraction pattern intensity equal to the modulus square of the Fourier Transform (FT) $\tilde{\rho}(\mathbf{k})$:

$$I(\mathbf{k}) = |\tilde{\rho}(\mathbf{k})|^2 \quad (1)$$

where \mathbf{k} represent the coordinate in the Fourier (or Reciprocal) space. In absence of constraints, any phase $\varphi(\mathbf{k})$ can be applied to form our solution $\tilde{\rho} = \sqrt{I}e^{i\varphi}$.

Phase retrieval consists in solving (Eq. (1)) from the measured intensity values $I(\mathbf{k})$ and some other prior knowledge (constraints). Diffraction microscopy solves the phase problem using the knowledge that the object

*Current address: Lawrence Berkeley National Laboratory, 1 Cyclotron Rd, Berkeley CA 94720, USA. e-mail: smarchesini@lbl.gov

being imaged is isolated, it is assumed to be 0 outside a region called support S :

$$\rho(\mathbf{r}) = 0, \text{ if } \mathbf{r} \notin S. \quad (2)$$

In practical experiments, where the object interacts by absorbing as well as refracting incident light, the problem is generalized to the most difficult case of objects with complex “density” or index of refraction. In case of complex objects, this “support” region is the only constraint and needs to be well defined, tightly wrapping the object. In many cases high contrast, sharp objects or illuminating beam boundaries are sufficient to obtain such support of the object ab-initio [6, 20].

A projection onto this set (\mathbf{P}_s) involves setting to 0 the components outside the support, while leaving the rest of the values unchanged:

$$\mathbf{P}_s \rho(\mathbf{r}) = \begin{cases} \rho(\mathbf{r}) & \text{if } \mathbf{r} \in S, \\ 0 & \text{otherwise.} \end{cases} \quad (3)$$

Its complementary projector can be expressed as $\mathbf{P}_{\bar{s}} = \mathbf{I} - \mathbf{P}_s$.

The projection to the nearest solution of (Eq. (1)) in reciprocal space is obtained by setting the modulus to the measured one $m(\mathbf{k}) = \sqrt{I(\mathbf{k})}$, and leaving the phase unchanged:

$$\tilde{\mathbf{P}}_m \tilde{\rho}(\mathbf{k}) = \tilde{\mathbf{P}}_m |\tilde{\rho}(\mathbf{k})| e^{i\varphi(\mathbf{k})} = \sqrt{I(\mathbf{k})} e^{i\varphi(\mathbf{k})}, \quad (4)$$

Singularities arise when $\tilde{\rho}$ is close to 0, and a small change in its value will project on a distant point. Such projector is a “diagonal” operator in Fourier space, acting element-by-element on each amplitude. When applied to real-space densities $\rho(\mathbf{r})$, it becomes non-local, mixing every element with a forward \mathcal{F} and inverse \mathcal{F}^{-1} Fourier transform:

$$\mathbf{P}_m = \mathcal{F}^{-1} \tilde{\mathbf{P}}_m \mathcal{F}. \quad (5)$$

The Euclidean length $\|\rho\|$ of a vector ρ is defined as:

$$\|\rho\|^2 = \rho^\dagger \cdot \rho = \sum_{\mathbf{r}} |\rho(\mathbf{r})|^2 = \sum_{\mathbf{k}} |\tilde{\rho}(\mathbf{k})|^2. \quad (6)$$

If some noise $\sigma(k)$ is present, the sum should be weighted by $w = \frac{1}{\sigma^2}$. The distance from the current point to the corresponding set $\|\mathbf{P}_s \rho - \rho\|$ is the basis for our error metrics:

$$\begin{aligned} \varepsilon_s(\rho) &= \|\mathbf{P}_s \rho - \rho\|, \\ \varepsilon_m(\rho) &= \|\mathbf{P}_m \rho - \rho\|, \end{aligned} \quad (7)$$

or their normalized version $\bar{\varepsilon}_{s,m}(\rho) = \frac{\varepsilon_{s,m}(\rho)}{\|\mathbf{P}_{s,m} \rho\|}$.

The gradients of the squared error metrics can be expressed in terms of projectors [10, 21]:

$$\nabla \varepsilon_m^2(\rho) = -2[\mathbf{P}_m - \mathbf{I}] \rho \quad (8)$$

$$\nabla \varepsilon_s^2(\rho) = -2[\mathbf{P}_s - \mathbf{I}] \rho, \quad (9)$$

Steps of $-\frac{1}{2} \nabla \varepsilon_{s,m}^2$ bring the corresponding error metrics to 0. The solution, hopefully unique, is obtained when both error metrics are 0.

3. Minimization in feasible space

One popular algorithm [10, 22] fits the data by minimizing the error metric $\varepsilon_m(\rho)$:

$$\begin{aligned} \min_{\rho} \varepsilon_m^2(\rho), \\ \text{subject to } \mathbf{P}_s \rho = 0, \end{aligned} \quad (10)$$

by enforcing the constraint and moving only in the feasible space $\rho_s = \mathbf{P}_s \rho$. The problem is transformed into an unconstrained optimization with a reduced set of variables ρ_s :

$$\min_{\rho_s} \varepsilon_m^2(\rho_s). \quad (11)$$

The steepest descent direction is projected in the feasible space:

$$\begin{aligned} \rho^{(n+1)} &= \rho^{(n)} + \Delta \rho^{(n)}, \\ \Delta \rho^{(n)} &= -\frac{1}{2} \nabla_s \varepsilon_m^2(\rho^{(n)}), \\ &= -\mathbf{P}_s [\mathbf{I} - \mathbf{P}_m] \rho^{(n)}, \end{aligned} \quad (12)$$

where $\nabla_s = \mathbf{P}_s \nabla$ is the component of the gradient in the support. This algorithm is usually written as a projection algorithm:

$$\rho^{(n+1)} = \mathbf{P}_s \mathbf{P}_m \rho^{(n)}; \quad (13)$$

by projecting back and forth between two sets, it converges to the local minimum. Such algorithm is commonly referred to as Error Reduction (ER) in the phase retrieval community [10].

Notice that a step of $-\frac{1}{2} \nabla \varepsilon_m^2(\rho)$ brings the error $\varepsilon_m^2(\rho)$ to 0. By projecting this step, setting to 0 some of its components, we reduce the step length. Typically [12, 23] the optimal step is longer than this step, we can move along this direction and minimize further the error metric. The simplest acceleration strategy, the steepest descent method, performs a line search of the local minimum in the steepest descent direction:

$$\min_{\delta} \varepsilon_m^2(\rho + \delta \Delta \rho). \quad (14)$$

At a minimum any further movement in the direction of the current step increases the error metric; the gradient direction must be perpendicular to the current step. In the steepest descent case, where the step is proportional to the gradient, the current step and the next become orthogonal:

$$\begin{aligned} \frac{\partial}{\partial \delta} \varepsilon_m^2(\rho + \delta \Delta \rho_s) &= \langle \Delta \rho_s | 2\mathbf{P}_s [\mathbf{I} - \mathbf{P}_m] (\rho + \delta \Delta \rho_s) \rangle_r, \\ 0 &= \langle \Delta \rho_s | [\mathbf{I} - \mathbf{P}_m] (\rho + \delta \Delta \rho_s) \rangle_r, \end{aligned} \quad (15)$$

where $\langle \mathbf{x} | \mathbf{y} \rangle_r = \Re(\mathbf{x}^\dagger \cdot \mathbf{y})$ and the projector \mathbf{P}_s is redundant and is removed. The line search algorithm can use ε_m^2 , and/or its derivative in (Eq. (15)). This optimization should be performed in reciprocal space, where the

modulus projector is fast to compute (Eq. (4)), while the support projection requires two Fourier transforms:

$$\tilde{P}_s = \mathcal{F}P_s\mathcal{F}^{-1}, \quad (16)$$

but it needs to be computed only once to calculate $\Delta\rho_s$.

The steepest descent method is known to be inefficient in the presence of long narrow valleys, where imposing that successive steps be perpendicular causes the algorithm to zig-zag down the valley. This problem is solved by the non-linear conjugate gradient method [24, 25, 26, 27, 28]. While error minimization methods converge to stable solutions quite rapidly however, the number of local minima is often too large for practical ab-initio phase retrieval applications and minimization methods are used only for final refinement.

4. Saddle-point optimization

The following algorithm is a reformulation of the HIO algorithm from a gradient/constraint perspective. We seek the saddle point of the error-metric difference $\mathcal{L}(\rho) = \varepsilon_m^2(\rho) - \varepsilon_s^2(\rho)$ [19]:

$$\min_{\rho_s} \max_{\rho_{\underline{s}}} \mathcal{L}(\rho_s + \rho_{\underline{s}}), \quad (17)$$

by moving in the steepest descent direction for ρ_s ($-\mathbf{P}_s\nabla$) and ascent direction ($+\mathbf{P}_{\underline{s}}\nabla$) for $\rho_{\underline{s}}$. For reasons discussed in appendix (A), we reduce the $\tilde{\mathbf{P}}_{\underline{s}}$ component by a relaxation parameter $\beta \in [0.5, 1]$:

$$\Delta\rho^{(n)} = \{-\mathbf{P}_s + \beta\tilde{\mathbf{P}}_{\underline{s}}\}\frac{1}{2}\nabla\mathcal{L}(\rho^{(n)}). \quad (18)$$

The gradient of \mathcal{L} (from Eqs. (8,9)):

$$\nabla\mathcal{L}(\rho) = 2[\mathbf{P}_s - \mathbf{P}_m]\rho, \quad (19)$$

is used in Eq. (18) to express the step and the new iteration point $\rho^{(n+1)}$ as:

$$\begin{aligned} \Delta\rho^{(n)} &= \{\mathbf{P}_s[\mathbf{P}_m - \mathbf{I}] - \beta\tilde{\mathbf{P}}_{\underline{s}}\mathbf{P}_m\}\rho^{(n)}, \\ \rho^{(n+1)} &= [\mathbf{P}_s\mathbf{P}_m + \tilde{\mathbf{P}}_{\underline{s}}[\mathbf{I} - \beta\mathbf{P}_m]]\rho^{(n)}. \end{aligned} \quad (20)$$

This iteration can be expressed in a more familiar form of the HIO algorithm [9, 10]:

$$\rho^{(n+1)}(\mathbf{r}) = \begin{cases} \mathbf{P}_m\rho^{(n)}(\mathbf{r}) & \text{if } \mathbf{r} \in S, \\ (\mathbf{I} - \beta\tilde{\mathbf{P}}_{\underline{s}})\rho^{(n)}(\mathbf{r}) & \text{otherwise.} \end{cases} \quad (21)$$

Rather than setting to 0 the object $\rho(\mathbf{r})$ where it is known to be 0 ($\mathbf{r} \notin S$), this algorithm seeks a stable condition of a feedback system in which the nonlinear operator \mathbf{P}_m provides the feedback term $\mathbf{P}_{\underline{s}}\mathbf{P}_m\rho$. From a fixed point whereby the feedback is 0 but the constraint is violated ($\mathbf{P}_{\underline{s}}\rho \neq 0$) it is often possible to obtain a solution by a simple projection $\mathbf{P}_m\rho$ [13]. In fact $\mathbf{P}_m\rho$ often satisfies the constraints better than the current iteration ρ , as the algorithm tries to escape a local minimum.

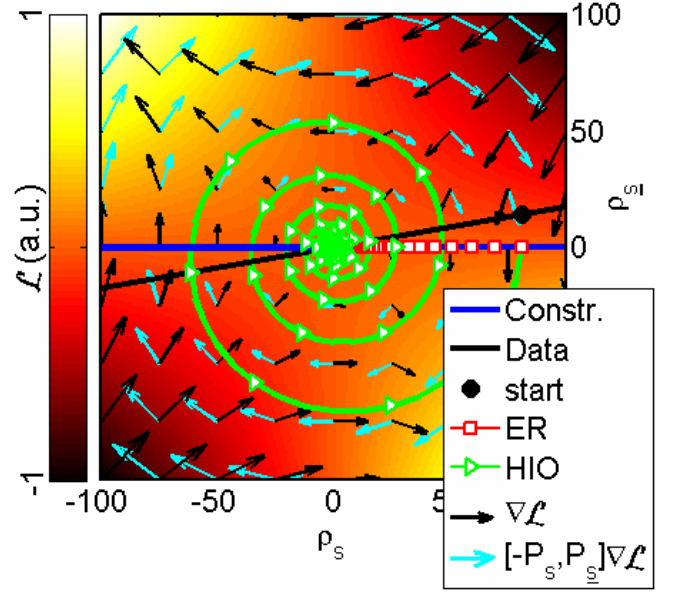


Fig. 1. Algorithms seek the intersection between two sets (data and constraints represented by two lines) using different types of fixed points: ER projects back and forth between the two sets, moving toward the minimum of ε_m within the constraint (horizontal line). HIO seeks the saddle point ($\min_s \max_{\underline{s}}$) of (\mathcal{L}), represented in background in pseudocolormap. \mathcal{L} is the difference of the square distances (ε^2) between the current point and the two sets. The gradient ($\nabla\mathcal{L}$) is indicated by black arrows. In order to reach the saddle point, HIO spirals toward the solution by inverting the gradient component parallel to the constraint (horizontal direction) following a descent-ascent direction ($[-\mathbf{P}_s + \mathbf{P}_{\underline{s}}]\nabla\mathcal{L}$ in light blue) toward the solution. Marker symbols are plotted every 5 iterations. See also [19] for a comparison with other algorithms.

In the steepest descent method, optimization of the step length is obtained by increasing a multiplication factor δ until the current and next search directions become perpendicular to one another:

$$\langle \Delta\rho | [-\mathbf{P}_s + \beta\tilde{\mathbf{P}}_{\underline{s}}]\nabla\mathcal{L}(\rho + \delta\Delta\rho) \rangle_r = 0. \quad (22)$$

A more robust strategy involves replacing the one dimensional search with a two dimensional optimization of the saddle point:

$$\min_{\alpha} \max_{\beta} \psi(\alpha, \beta),$$

$$\psi(\alpha, \beta) = \mathcal{L}(\rho + \alpha\Delta\rho_s + \beta\Delta\rho_{\underline{s}}), \quad (23)$$

$$\Delta\rho_s = -\frac{1}{2}\nabla_s\mathcal{L}(\rho); \Delta\rho_{\underline{s}} = \frac{1}{2}\nabla_{\underline{s}}\mathcal{L}(\rho); \quad (24)$$

where both components ($\mathbf{P}_s, \mathbf{P}_{\underline{s}}$) of successive steps are perpendicular to one another:

$$\begin{aligned} \frac{\partial\psi}{\partial\alpha} &= \langle \Delta\rho_s | \nabla\mathcal{L}(\rho + \alpha\Delta\rho_s + \beta\Delta\rho_{\underline{s}}) \rangle_r = 0, \\ \frac{\partial\psi}{\partial\beta} &= \langle \Delta\rho_{\underline{s}} | \nabla\mathcal{L}(\rho + \alpha\Delta\rho_s + \beta\Delta\rho_{\underline{s}}) \rangle_r = 0. \end{aligned} \quad (25)$$

This two dimensional minmax problem needs to be fast to provide real acceleration, and will be discussed in the following section.

5. Two dimensional subproblem

The local saddle point (Eq. (23)) requires two conditions to be met. The first order condition is that the solution is a stationary (or fixed) point, where the gradient of ψ is 0 (Eq. (25)). We rewrite the condition in a compact form:

$$\nabla_{\tau}\psi(\tau) = \langle \Delta\rho | \nabla_{\rho}\mathcal{L}(\rho + \tau^T \Delta\rho) \rangle_{\tau} = 0, \quad (26)$$

$$\tau = \begin{pmatrix} \alpha \\ \beta \end{pmatrix}, \Delta\rho = \begin{pmatrix} \Delta\rho_s \\ \Delta\rho_{\underline{s}} \end{pmatrix}, \nabla_{\rho} = \begin{pmatrix} \nabla_s \\ \nabla_{\underline{s}} \end{pmatrix}. \quad (27)$$

At the origin ($\tau = 0$), the gradient $\nabla_{\tau}\psi$ is negative in the \mathbf{P}_s subspace and positive in the $\mathbf{P}_{\underline{s}}$ subspace, decreasing (increasing) \mathcal{L} in the steepest descent (ascent) directions in the two orthogonal spaces:

$$\begin{aligned} \nabla_{\tau}\psi(0) &= \begin{pmatrix} \Delta\rho_s | \nabla_s \mathcal{L}(\rho) \rangle \\ \Delta\rho_{\underline{s}} | \nabla_{\underline{s}} \mathcal{L}(\rho) \rangle \end{pmatrix}, \\ &= 2 \begin{pmatrix} -||\Delta\rho_s||^2 \\ +||\Delta\rho_{\underline{s}}||^2 \end{pmatrix} = \frac{1}{2} \begin{pmatrix} -||\nabla_s \mathcal{L}(\rho)||^2 \\ +||\nabla_{\underline{s}} \mathcal{L}(\rho)||^2 \end{pmatrix}. \end{aligned} \quad (28)$$

The minimal residual method finds a stationary point by minimizing the norm of the gradient:

$$\min_{\tau} \Phi(\tau), \quad \Phi = \frac{1}{2} ||\nabla_{\tau}\psi(\tau)||^2, \quad (29)$$

transforming the saddle point problem in a minimization problem, and providing the metric Φ to monitor progress. However this method can move to other stationary points.

Second order conditions (min-max) require the Hessian \mathcal{H} of ψ (the Jacobian of (Eq. (26)) to be symmetric and indefinite (neither positive nor negative definite):

$$\mathcal{H}_{\tau} = \begin{pmatrix} \partial_{\alpha}\partial_{\alpha} & \partial_{\alpha}\partial_{\beta} \\ \partial_{\beta}\partial_{\alpha} & \partial_{\beta}\partial_{\beta} \end{pmatrix} \psi, \begin{cases} \mathcal{H}_{\alpha,\alpha} \geq 0, \\ \mathcal{H}_{\beta,\beta} \leq 0. \end{cases} \quad (30)$$

This Hessian is computed analytically (see appendix (B)), it is small (2×2), and can be used to compute the Newton step:

$$\Delta\tau = -\mathcal{H}^{-1} \nabla_{\tau}\psi. \quad (31)$$

However, the Hessian precise value is not necessary and requires an effort that could be avoided by other methods.

The normalized steepest descent-ascent (SDA) direction can be expressed in terms of a Newton step using an approximate diagonal Hessian whose elements are equal to $-\nabla\psi(0)$:

$$\hat{\mathcal{H}}^{\text{SDA}} = 2 \begin{pmatrix} ||\Delta\rho_s||^2 & 0 \\ 0 & -||\Delta\rho_{\underline{s}}||^2 \end{pmatrix}. \quad (32)$$

The Hessians $\hat{\mathcal{H}}$ satisfies condition (Eq. (30)), ensuring that $\Delta\tau$ is less then 90° from the direction of the saddle.

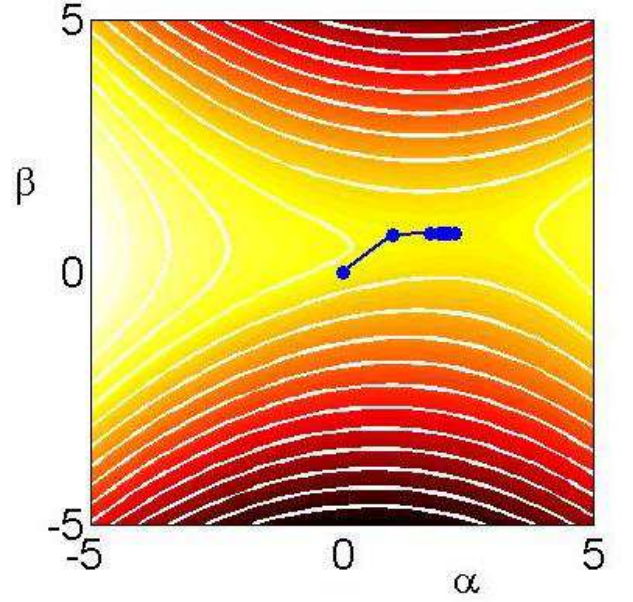


Fig. 2. Pseudocolor and contour maps of the lower dimensional function $\psi(\alpha, \beta)$ are depicted in the background. This ψ was computed from one iteration of the test described in Sec. (6). The saddle, typical of this test, is wide in the horizontal direction and narrow in the vertical, showing the importance of the relaxation parameter $\bar{\beta} < 1$ to reduce (precondition) the vertical move. However, the condition number increases near the saddle-point as it becomes even narrower in the vertical direction. Often the dependence of ψ with respect to the fitting parameter β (vertical axis) resembled a v centered near the solution, and successive iterations using just a preconditioner jumped up and down near the saddle-point. Iterations using the SR1 quasi-Newton update (starting from $\tau^{(0)} = 0$, $\mathcal{H}^{(0)} = \hat{\mathcal{H}}^{\text{HIO}}$) shown here converge rapidly to the solution.

Starting from $\tau^{(0)} = \mathbf{0}$, the first iteration gives a unit step $\tau^{(1)} = -\hat{\mathcal{H}}^{-1} \nabla\psi(\mathbf{0}) = \begin{pmatrix} 1 \\ 1 \end{pmatrix}$. A preconditioner can be used to reduce the feedback:

$$\hat{\mathcal{H}}^{\text{HIO}} = \begin{pmatrix} 1 & 0 \\ 0 & 1/\bar{\beta} \end{pmatrix} \hat{\mathcal{H}}^{\text{SDA}}, \quad (33)$$

providing the HIO step at the first iteration, $\tau^{(1)} = \Delta\tau^{(0)} = \begin{pmatrix} 1 \\ \bar{\beta} \end{pmatrix}$. This approximate Hessian can be used as a starting guess, which is often all it is needed to achieve fast convergence.

We can perform a line search using the preconditioner $\hat{\mathcal{H}}^{-1}$:

$$\langle \Delta\tau | \hat{\mathcal{H}}^{-1} \nabla_{\tau}\psi(\tau + \delta\Delta\tau) \rangle_{\tau} = 0. \quad (34)$$

However the Hessian of $\hat{\mathcal{H}}^{-1}\psi$ is antisymmetric, the algorithm is unstable and could spiral away from the solution. The bi-conjugate gradient method applies to symmetric indefinite Hessians and monitors progress of the

algorithm. Conjugate directions $\Lambda\tau$ replace the steepest descent direction in the line search (with $\gamma^{(0)} = 0$):

$$\begin{aligned}\Lambda\tau^{(n+1)} &= \Delta\tau^{(n+1)} + \gamma^{(n)}\Lambda\tau^{(n)}, \\ \gamma^{(n)} &= \frac{\langle \Delta\tau^{(n+1)} | \hat{\mathcal{H}}^{(-1)} (\nabla\psi(\tau^{(n+1)}) - \nabla\psi(\tau^{(n)})) \rangle}{\langle \Delta\tau^{(n)} | \hat{\mathcal{H}}^{-1} \Delta\psi(\tau^{(n)}) \rangle}.\end{aligned}\quad (35)$$

A better option is to use a quasi-Newton update of the Hessian or its inverse (a secant method in higher dimensions) based on the new gradient values. The *Symmetric Rank 1* (SR1) method can be applied to indefinite problems [29]:

$$\begin{aligned}\mathbf{y} &= \nabla\tau\psi(\tau + \Delta\tau) - \nabla\tau\psi(\tau), \\ \Delta\mathcal{H}^{-1} &= \frac{\|\Delta\tau - \mathcal{H}^{-1}\mathbf{y}\|^2}{(\Delta\tau - \mathcal{H}^{-1}\mathbf{y})^T \cdot \mathbf{y}}, \\ \mathcal{H}^{-1} &\rightarrow \mathcal{H}^{-1} + \Delta\mathcal{H}^{-1}.\end{aligned}\quad (36)$$

Second order conditions (Eq. (30)) can be imposed to the Hessian, by flipping the sign or setting to 0 the values that violate them. Φ can be used to monitor progress, as long as we are in the neighborhood of the solution and the Hessian satisfies second order conditions (Eq. (30)). It was found that the Hessian and step size parameters were fairly constant for each 2D optimization, therefore the first guess for τ and \mathcal{H} was obtained from the average of the previous 5 of such optimizations. With such initial guess, 3 SR1 iterations of the lower dimensional problem were often sufficient to reduce Φ below a threshold of 0.01 $\Phi(0)$ in the tests described below.

In summary, an efficient algorithm is obtained by a combination of HIO/quasi-Newton/Newton methods with a trust region $|\Delta\tau| \leq r$:

1. calculate step $\Delta\rho = -\frac{1}{2} \begin{pmatrix} \nabla_s \mathcal{L} \\ -\nabla_{\mathbf{z}} \mathcal{L} \end{pmatrix}$, and set trust region radius $r = r_{\max}$.
2. if the iteration number is ≤ 5 , use HIO as first guess: $\mathcal{H} = \hat{\mathcal{H}}^{\text{HIO}}$, $\tau^{(1)} = (1, \bar{\beta})$.
3. otherwise average 5 previous optimized step sizes τ , and Hessians \mathcal{H} , and use the average as initial guess.
4. calculate gradient $\nabla\psi(\tau)$. If small, exit loop (go to 10).
5. compute Newton step using approximate Hessian: $\Delta\tau = -\mathcal{H}^{-1}\nabla\psi$, enforce trust region $|\Delta\tau| < r$.
6. update inverse Hessian with SR1 method (Eq. 36).
7. if the Hessian error $\|\Delta\tau - \mathcal{H}^{-1}\mathbf{y}\|^2$ is too large, calculate the true Hessian, perform a line search, decrease trust region radius r .
8. force Hessian to satisfy second order conditions (Eq. 30), by changing the sign of the values that violate conditions.



Fig. 3. Test figure used for benchmarking (total size: 256^2 , object size: 128^2 pixels. The support was slightly larger than the object: 129^2 pixels).

9. update $\tau \rightarrow \tau + \Delta\tau$ and go back to 4.

10. update $\rho \rightarrow \rho + \tau^T \Delta\rho$. If $\bar{\varepsilon}_m$ is small exit, otherwise go back to 1.

The trust region is used to obtain a more robust algorithm, is reset at each inner loop, it increases if things are going well, decreases if the iteration is having trouble, but it is kept between (r_{\min}, r_{\max}) , typically (0.5, 3). We can keep track of $\tau, \nabla\tau$ computed, and restart the algorithm once in a while from the root of the 2D linear fit of $\nabla\psi(\tau)$.

We can easily extend this algorithm to two successive steepest descent-ascent directions, by performing a higher dimensional (4D) saddle-point optimization:

$$\min_{\alpha^{(n,n+1)}} \max_{\beta^{(n,n+1)}} \mathcal{L} \left(\rho + (\tau^{(n+1)})^T \Delta\rho^{(n+1)} + (\tau^{(n)})^T \Delta\rho^{(n)} \right)$$

This 4D optimization is performed using the same Newton/quasi-Newton trust-region optimization as in the 2D case. The first step $(\tau^0)^T \Delta\rho^0$ is obtained solving the 2D minmax problem, and the following ones will be perpendicular to the last 2 iterations.

6. Performance tests

The tests presented here were combined with other algorithms in [19]. In such comparison between algorithms, the original HIO algorithm performed better than other algorithms described in the literature. Fig. 3 was used to simulate a diffraction pattern, and several phase retrieval tests were performed using different random starts. When applying a nonnegativity constraint HIO always converged within a few hundred iterations. The algorithms were therefore tested using a more difficult problem, nonnegativity and reality constraints were removed, allowing the reconstructed image to be complex, adding many degrees of freedom within the constraint.

When the error metric ε_m fell below a threshold it was considered a successful reconstruction. The threshold 10^{-4} chosen was enough to obtain visually good reconstructions.

Fig. 4 shows the relative performance of the various algorithms. By adding 2D or 4D optimization, the algorithm converged more reliably and in less iterations

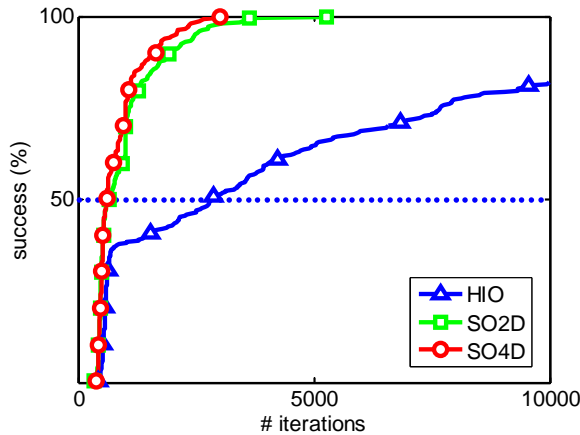


Fig. 4. Successful phase retrievals, starting from random phases, as a function of iterations. When the normalized error metric $\bar{\epsilon}_m$ falls below a threshold (10^{-4}) it is considered a successful reconstruction. The plot represents the cumulative sum of the number of successful reconstructions vs the number of iterations required. Values for 50% (dotted line) and 100% success are listed in Tab. 1. Comparison with other algorithms is shown in [19].

Table 1. Benchmark of various algorithms (250 trials) summarizing the results in Fig. 4.

Algorithm	No. of iterations for		success rate (total)
	50% success	100% success	
HIO	2790	> 10000	82%
SO2D	656	5259	100%
SO4D	605	2999	100%

to a solution (Table 1). The 2D (and 4D) optimization, written in an upper-level language (matlab) increased the computational time of each iteration by a factor of 3 (and 4) and required the storage 2 (and 4) additional matrices compared to HIO. HIO itself requires 2 matrices in addition to the data and constraints. A c-code version of the algorithm developed by F. Maia from U. Uppsala performed slightly faster, and could be further optimized by reducing some of the redundant computations involved.

This lower dimensional optimization employs matrix cross products, computing a number of floating point operations proportional to the number of elements of the images (and can be implemented on parallel systems). The Fourier transforms employed to calculate the steps in the higher dimensional problem will dominate the computational burden for larger matrices.

7. Conclusions

The hybrid input-output method, usually described as a projection algorithm, is a remarkable method to solve nonconvex phase problems. When written as a saddle point problem, HIO speed and reliability can be improved

by applying Newton methods to explore lower dimensional search directions. This approach differs from other nonlinear optimization algorithms that try to satisfy constraints using various forms of barriers or trust regions, often requiring stochastic methods to climb out of local minima present in nonconvex problems.

The saddle-point algorithm, while following a path indicated by a gradient, does not seek a minimum and does not stop at local minima. Although stagnation occurs, it appears that the area of convergence to the global solution is much larger compared to simple minimization methods. Problems arise at the locations of 0 intensity values where phase singularities occur, causing optimization problems to be nonsmooth. Various forms of preconditioning low intensity values could be applied to this problem [30, 31], here the nonsmooth behavior of the problem is addressed using a lower dimensional optimization to stabilize the iterations, providing a more reliable algorithm.

In this paper, the saddle-point optimization was performed for a simple equality constraint $\mathbf{P}_s \rho = 0$. Such linear constraint allows rapid calculation of the gradients involved in the lower dimensional optimization. Linear approximation or more advanced methods could be applied to other nonlinear constraints such as thresholds, histograms, atomicity and object connectivity, extending this approach to a larger class of problems. This saddle-point optimization formalism can easily be generalized to other problems of conflicting requirements where gradients or projections can be computed.

Appendix A: Relaxation parameter and phase singularities

The large dimensional minmax problem (Eq. 17) can be expressed in a system of two parts:

$$\begin{cases} \min_{\rho_s} \epsilon_m^2(\rho) = \min_{\rho_s} \|\mathbf{I} - \mathbf{P}_m\| \rho \|^2 \\ \min_{\rho_s} \epsilon_s^2(\rho) - \epsilon_m^2(\rho) = \min_{\rho_s} 2\langle \mathbf{P}_m \rho | \rho \rangle_r + c \end{cases} \quad (\text{A1})$$

The upper optimization is similar to the problem treated in Section 3, converging to a local minimum with a simple projected gradient method. The lower function, however, can be discontinuous in the presence of zeros ($\tilde{\rho}_s = 0$) in Fourier space:

$$\langle \tilde{\mathbf{P}}_m \tilde{\rho} | \tilde{\rho} \rangle = \sum \sqrt{I} |\tilde{\rho}_s + \tilde{\rho}_s| \quad (\text{A2})$$

which is a non-smooth v-shaped function of $\tilde{\rho}_s$ for $\tilde{\rho}_s = 0$, $\sqrt{I} > 0$, and simple gradient methods oscillate around minima. The projected gradient step can be overestimated and requires the relaxation parameter $\tilde{\beta}$. Zeros in Fourier space are candidates (necessary but not sufficient condition) for the location of phase vortices, phase discontinuities, which are known to cause stagnation [33]. Analytical [32], statistical [3, 33, 34], and deterministic [30, 31] methods have been proposed to overcome such singularities.

Appendix B: Two dimensional gradient and Hessian

The function \mathcal{L} in reciprocal space can be expressed as:

$$\begin{aligned}\mathcal{L}(\tilde{\rho}_s + \tilde{\rho}_{\underline{s}}) &= \left\| [\mathbf{I} - \tilde{\mathbf{P}}_m](\tilde{\rho}_s + \tilde{\rho}_{\underline{s}}) \right\|^2 - \left\| \tilde{\rho}_{\underline{s}} \right\|^2 \quad (\text{B1}) \\ &= \sum |\tilde{\rho}_s|^2 - 2\sqrt{I}|\tilde{\rho}_s + \tilde{\rho}_{\underline{s}}| + \sqrt{I}.\end{aligned}$$

and the two components of the gradients:

$$\nabla \mathcal{L} = \begin{pmatrix} \mathbf{P}_s \nabla \mathcal{L} \\ \mathbf{P}_{\underline{s}} \nabla \mathcal{L} \end{pmatrix} = 2 \begin{pmatrix} \mathbf{P}_s [\mathbf{I} - \mathbf{P}_m](\rho_s + \rho_{\underline{s}}) \\ -\mathbf{P}_{\underline{s}} \mathbf{P}_m(\rho_s + \rho_{\underline{s}}) \end{pmatrix} \quad (\text{B2})$$

The corresponding steps $\Delta \rho_s = -\frac{1}{2}\nabla_s \mathcal{L}$, $\Delta \rho_{\underline{s}} = +\frac{1}{2}\nabla_{\underline{s}} \mathcal{L}$.

The function $\psi(\alpha, \beta)$ can be calculated in reciprocal space, provided that the components $\tilde{\rho}_{s,\underline{s}}$, $\Delta \tilde{\rho}_{s,\underline{s}}$ are known:

$$\begin{aligned}\psi(\alpha, \beta) &= \left\| [\mathbf{I} - \tilde{\mathbf{P}}_m] (\tilde{\rho} + \alpha \Delta \tilde{\rho}_s + \beta \Delta \tilde{\rho}_{\underline{s}}) \right\|^2 \\ &\quad - \left\| \tilde{\rho}_{\underline{s}} + \beta \Delta \tilde{\rho}_{\underline{s}} \right\|^2 \\ &= \sum_{\mathbf{k}} \left| \tilde{\rho} + \alpha \Delta \tilde{\rho}_s + \beta \Delta \tilde{\rho}_{\underline{s}} - \sqrt{I} \right|^2 \\ &\quad - \left| \tilde{\rho}_{\underline{s}} + \beta \Delta \tilde{\rho}_{\underline{s}} \right|^2 \\ &= \sum_{\mathbf{k}} I + |\tilde{\rho}_s + \alpha \Delta \tilde{\rho}_s|^2 \\ &\quad - 2\sqrt{I} |\tilde{\rho} + \alpha \Delta \tilde{\rho}_s + \beta \Delta \tilde{\rho}_{\underline{s}}| \quad (\text{B3})\end{aligned}$$

The gradient components (writing $\tilde{\rho}_\tau = \tilde{\rho} + \boldsymbol{\tau}^T \boldsymbol{\Delta} \tilde{\rho} = \tilde{\rho} + \alpha \Delta \tilde{\rho}_s + \beta \Delta \tilde{\rho}_{\underline{s}}$) are:

$$\begin{aligned}\nabla_{\mathbf{t}} \psi &= \langle \boldsymbol{\Delta} \tilde{\rho} | \nabla \mathcal{L}(\tilde{\rho}_\tau) \rangle_r, \quad (\text{B4}) \\ &= 2 \langle \boldsymbol{\Delta} \tilde{\rho} | [\tilde{\mathbf{P}}_s - \tilde{\mathbf{P}}_m] \tilde{\rho}_\tau \rangle_r, \\ \frac{\partial \psi}{\partial \alpha} &= 2 \langle \Delta \tilde{\rho}_s | [\mathbf{I} - \tilde{\mathbf{P}}_m] \tilde{\rho}_\tau \rangle_r, \\ \frac{\partial \psi}{\partial \beta} &= 2 \langle \Delta \tilde{\rho}_{\underline{s}} | [-\tilde{\mathbf{P}}_m] \tilde{\rho}_\tau \rangle_r,\end{aligned}$$

Using common derivative rules:

$$\frac{\partial}{\partial x} |x| = \frac{x}{|x|}, \quad (\text{B5})$$

$$\frac{\partial}{\partial \alpha} |x + \alpha \Delta x| = \frac{\Re(\Delta x^\dagger (x + \alpha \Delta x))}{|x + \alpha \Delta x|}, \quad (\text{B6})$$

$$\begin{aligned}\frac{\partial}{\partial \alpha} \frac{x + \alpha \Delta x}{|x + \alpha \Delta x|} &= \frac{\Delta x}{|x + \alpha \Delta x|} - \frac{x + \alpha \Delta x}{|x + \alpha \Delta x|^3} \\ &\quad \cdot \frac{\Re(\Delta x^\dagger (x + \alpha \Delta x))}{|x + \alpha \Delta x|^2}, \quad (\text{B7})\end{aligned}$$

$$\frac{\partial}{\partial \alpha} |x + \alpha \Delta x|^2 = 2\Re(\Delta x^\dagger (x + \alpha \Delta x)), \quad (\text{B8})$$

$$\frac{\partial^2}{\partial \alpha^2} |x + \alpha \Delta x| = \frac{|\Delta x|^2}{|x + \alpha \Delta x|} - \frac{\Re(\Delta x^\dagger (x + \alpha \Delta x))^2}{|x + \alpha \Delta x|^3}, \quad (\text{B9})$$

$$\frac{\partial^2}{\partial \alpha^2} |x + \alpha \Delta x|^2 = |\Delta x|^2, \quad (\text{B10})$$

and

$$\begin{aligned}\frac{\partial^2 |x + \alpha \Delta x + \beta \Delta y|}{\partial \alpha \partial \beta} &= \frac{\Re(\Delta x^\dagger \Delta y)}{|x + \alpha \Delta x + \beta \Delta y|} \\ &\quad - \frac{\Re(\Delta x^\dagger (x + \alpha \Delta x + \beta \Delta y))}{|x + \alpha \Delta x + \beta \Delta y|} \\ &\quad \cdot \frac{\Re(\Delta y^\dagger (x + \alpha \Delta x + \beta \Delta y))}{|x + \alpha \Delta x + \beta \Delta y|^2}, \quad (\text{B11})\end{aligned}$$

we can calculate the analytic expression for the Hessian using $\tilde{\mathbf{P}}_m \tilde{\rho} = \frac{\tilde{\rho}}{|\tilde{\rho}|} \sqrt{I}$. Starting from the simplest component:

$$\begin{aligned}\frac{\partial^2 \psi}{\partial \beta^2} &= -2 \left\langle \Delta \tilde{\rho}_{\underline{s}} \left| \frac{\partial \tilde{\mathbf{P}}_m \tilde{\rho}_\tau}{\partial \beta} \right. \right\rangle \quad (\text{B12}) \\ &= 2 \sum -\frac{|\Delta \tilde{\rho}_{\underline{s}}|^2 \sqrt{I}}{|\tilde{\rho}_\tau|} + \frac{\Re(\Delta \tilde{\rho}_{\underline{s}}^\dagger \tilde{\rho}_\tau)^2 \sqrt{I}}{|\tilde{\rho}_\tau|^3} \\ &= 2 \sum -\frac{|\Delta \tilde{\rho}_{\underline{s}}|^2 \sqrt{I}}{|\tilde{\rho}_\tau|} + \frac{\sqrt{I}}{2|\tilde{\rho}_\tau|} \frac{\Re(\Delta \tilde{\rho}_{\underline{s}}^\dagger \tilde{\rho}_\tau)(\Delta \tilde{\rho}_{\underline{s}}^\dagger \tilde{\rho}_\tau + \Delta \tilde{\rho}_{\underline{s}} \tilde{\rho}_\tau^\dagger)}{|\tilde{\rho}_\tau|^2} \\ &= 2 \left\langle \Delta \tilde{\rho}_{\underline{s}} \left| -\frac{\sqrt{I}}{2|\tilde{\rho}_\tau|} \left(1 - \frac{\tilde{\rho}_\tau^2}{\Delta \tilde{\rho}_{\underline{s}}^2} \frac{|\Delta \tilde{\rho}_{\underline{s}}|^2}{|\tilde{\rho}_\tau|^2} \right) \right| \Delta \tilde{\rho}_{\underline{s}} \right\rangle_r\end{aligned}$$

$$\begin{aligned}\frac{\partial^2 \psi}{\partial \alpha^2} &= 2 \left\langle \Delta \tilde{\rho}_s \left| \frac{\partial [\mathbf{I} - \tilde{\mathbf{P}}_m] \tilde{\rho}_\tau}{\partial \alpha} \right. \right\rangle_r, \quad (\text{B13}) \\ &= 2 \sum |\Delta \tilde{\rho}_s|^2 - \frac{|\Delta \tilde{\rho}_s|^2 \sqrt{I}}{|\tilde{\rho}_\tau|} + \frac{\Re(\Delta \tilde{\rho}_s^\dagger \tilde{\rho}_\tau)^2 \sqrt{I}}{|\tilde{\rho}_\tau|^3} \\ &= 2 \left\langle \Delta \tilde{\rho}_s \left| \left[1 - \frac{\sqrt{I}}{2|\tilde{\rho}_\tau|} \left(1 - \frac{\tilde{\rho}_\tau^2}{\Delta \tilde{\rho}_s^2} \frac{|\Delta \tilde{\rho}_s|^2}{|\tilde{\rho}_\tau|^2} \right) \right] \right| \Delta \tilde{\rho}_s \right\rangle_r\end{aligned}$$

The cross terms:

$$\begin{aligned}\frac{\partial^2 \psi}{\partial \beta \partial \alpha} &= 2 \left\langle \Delta \tilde{\rho}_s \left| \frac{\partial [\mathbf{I} - \tilde{\mathbf{P}}_m] \tilde{\rho}_\tau}{\partial \beta} \right. \right\rangle \quad (\text{B14}) \\ &= 2 \left\langle \Delta \tilde{\rho}_s \left| -\frac{\sqrt{I}}{2|\tilde{\rho}_\tau|} \left(1 - \frac{\tilde{\rho}_\tau^2}{\Delta \tilde{\rho}_s^2} \frac{|\Delta \tilde{\rho}_s|^2}{|\tilde{\rho}_\tau|^2} \right) \right| \Delta \tilde{\rho}_{\underline{s}} \right\rangle_r \\ &= 2 \left\langle \Delta \tilde{\rho}_{\underline{s}} \left| -\frac{\sqrt{I}}{2|\tilde{\rho}_\tau|} \left(1 - \frac{\tilde{\rho}_\tau^2}{\Delta \tilde{\rho}_s^2} \frac{|\Delta \tilde{\rho}_s|^2}{|\tilde{\rho}_\tau|^2} \right) \right| \Delta \tilde{\rho}_s \right\rangle_r.\end{aligned}$$

Acknowledgments

This work was performed under the auspices of the U.S. Department of Energy by the Lawrence Livermore National Laboratory under Contract No. W-7405-ENG-48 and the Director, Office of Energy Research. This work was partially funded by the National Science Foundation through the Center for Biophotonics, University of California, Davis, under Cooperative Agreement No. PHY0120999. F. Maia from Univ. of Uppsala for porting the code in c.

References

1. J. Miao, P. Charalambous, J. Kirz, D. Sayre, *Nature* **400**, 342 (1999).
2. D. Shapiro, P. Thibault, T. Beetz, V. Elser, M. Howells, C. Jacobsen, J. Kirz, E. Lima, H. Miao, A. Neiman, D. Sayre, *PNAS* **102** (43), 1543 (2005).
3. J. Miao, C-C. Chen, C. Song, Y. Nishino, Y. Kohmura, T. Ishikawa, D. Ramunno-Johnson, T-K. Lee, and S. H. Risbud, *Phys. Rev. Lett.* **97**, 215503 (2006).
4. M. A. Pfeifer, G. J. Williams, I. A. Vartanyants, R. Harder & I. K. Robinson, *Nature* **442**, 63-67 (2006).
5. A. Barty et al., "Three-dimensional ceramic nanofoam lattice structure determination using coherent X-ray diffraction imaging: insights into deformation mechanisms", submitted.
6. H. N. Chapman, A. Barty, S. Marchesini, A. Noy, C. Cui, M. R. Howells, R. Rosen, H. He, J. C. H.

- Spence, U. Weierstall, T. Beetz, C. Jacobsen, D. Shapiro, J. Opt. Soc. Am. A **23**, 1179-1200 (2006), (arXiv:physics/0509066).
7. H. N. Chapman, A. Barty, M. J. Bogan, S. Boutet, M. Frank, S. P. Hau-Riege, S. Marchesini, B. W. Woods, S. Bajt, W. H. Benner, R. A. London, E. Plönjes, M. Kuhlmann, R. Treusch, S. Düterer, T. Tschentscher, J. R. Schneider, E. Spiller, T. Möller, C. Bostedt, M. Hoener, D. A. Shapiro, K. O. Hodgson, D. Van Der Spoel, F. Burmeister, M. Bergh, C. Caleman, Gösta Huldt, M. M. Seibert, F. R. N. C. Maia, R. W. Lee, A. Szöke, N. Timneanu, Janos Hajdu, Nature Physics **2**, 789-862 (2006), (arxiv:physics/0610044).
8. P. W. Hawkes & J. C. H. Spence (Eds.), *Science of Microscopy* (Springer, 2007).
9. J. R. Fienup, Opt. Lett. **3**, 27-29 (1978).
10. J. R. Fienup, Appl. Opt. **21**, 2758-2769 (1982).
11. A. Levi and H. Stark, J. Opt. Soc. Am. A **1**, 932-943 (1984).
12. H. Stark, *Image Recovery: Theory and applications* (Academic Press, 1987).
13. V. Elser, J. Opt. Soc. Am. A **20**, 40-55 (2003).
14. H. H. Bauschke, P. L. Combettes, and D. R. Luke, J. Opt. Soc. Am. A **19**, 1334-1345 (2002).
15. H. H. Bauschke, P. L. Combettes, and D. R. Luke, J. Opt. Soc. Am. A **20**, 1025-1034 (2003).
16. D. R. Luke, Inverse Problems **21**, 37-50 (2005), (arXiv:math.OA/0405208).
17. V. Elser, I. Rankenburg, and P. Thibault, "Searching with iterated maps". Proc. Nat. Acc. Sci. **104**, 418-423 (2007).
18. V. Elser, I. Rankenburg, Phys. Rev. E **73**, 026702 (2006).
19. S. Marchesini, Rev. Sci. Inst. **78**, 011301 (2007), (arXiv:physics/0603201).
20. S. Marchesini et al. Phys. Rev. B **68**, (2003) 140101(R), (arXiv:physics/0306174).
21. D. R. Luke, J. V. Burke, R. G. Lyon, SIAM Review **44**, 169-224 (2002).
22. R. Gerchberg and W. Saxton, Optik **35**, 237-246 (1972).
23. D. C. Youla and H. Webb, "Image restoration by the method of projections onto convex sets. Part I," IEEE Trans. Med. Imaging TMI-1, 81-94 (1982).
24. M. R. Hestenes, *Conjugate Direction Methods in Optimization*, (Springer-Verlag, 1980).
25. W. H. Press, S. A. Teukolsky, W. T. Vetterling and B. P. Flannery, *Numerical Recipes in C* (Cambridge University Press, 1992).
26. M. J. D. Powell, Lecture Notes in Mathematics **1066**, 122-141 (1984).
27. E. Polak, *Computational Methods in Optimization* (Academic Press, 1971).
28. R. Fletcher, *Practical Methods of Optimization* (John Wiley & Sons, 2000).
29. J. Nocedal, S. J. Wright, *Numerical Optimization* (Springer Verlag, 2006).
30. T. Isernia, G. Leone, R. Pierri, and F. Soldovieri, J. Opt. Soc. Am. A **16**, 1845-1856 (1999).
31. G. Oszlányi and A. Süto, Acta Cryst. **A61**, 147-152 (2005).
32. P-T. Chen, M. A. Fiddy, C-W. Liao and D. A. Pommet, J. Opt. Soc. Am. A **13**, (1996), 1524-31.
33. J. R. Fienup, C. C. Wackerman, J. Opt. Soc. Am. A **3**, 1897-1907 (1986).
34. S. Marchesini, H. N. Chapman, A. Barty, M. R. Howells, J. C. H. Spence, C. Cui, U. Weierstall, and A. M. Minor, IPAP Conf. Series **7**, 380-382 (2006), (arXiv:physics/0510033).